UCRL-JC-132439
PREPRINT

Nonlinear Evolution of the Rayleigh-Taylor and Richtmyer-Meshkov Instabilities

G. Dimonte

This paper was prepared for submittal to the
American Physical Society 40th Annual Meeting of the
Division of Plasma Physics
New Orleans, LA
November 16-20, 1998

November 1, 1998

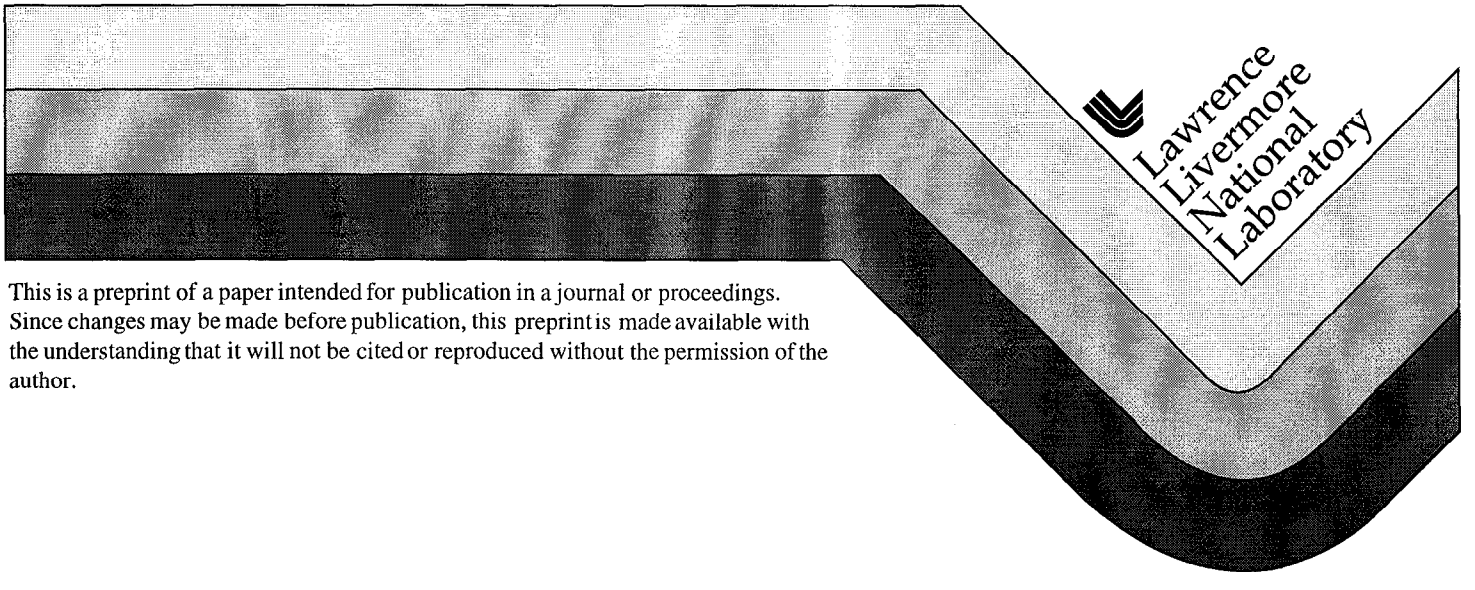

Nonlinear evolution of the Rayleigh-Taylor and Richtmyer-Meshkov instabilities

Guy Dimonte

Lawrence Livermore National Laboratory
Livermore, California 94551
November 9, 1998

ABSTRACT

Scaled experiments on the nonlinear evolution of the Rayleigh-Taylor (RT) and Richtmyer-Meshkov (RM) instabilities are described under a variety of conditions that occur in nature. At high Reynolds number, the mixing layer grows self-similarly ~ $\alpha_i Agt^2$ for a constant acceleration (g) and as a power law t^{θ_i} for impulsive accelerations $U\delta(t)$ at low and high Mach numbers. The growth coefficients α_i and θ_i exponents are measured over a comprehensive range of Atwood numbers A. The RT instability is also investigated with Non-Newtonian materials which are independently characterized. A critical wavelength and amplitude for instability is observed associated with the shear modulus and tensile yield of the material. The results are applicable from supernova explosions to geophysical flows subject to these hydrodynamic instabilities.

PACS numbers: 47.20.Bp, 47.25.Jn

1. Introduction

When a fluid of density ρ_1 accelerates another fluid of density ρ_2, hydrodynamic instabilities at the interface cause strong fluid mixing. The Rayleigh-Taylor [1] (RT) instability occurs for a sustained acceleration or buoyancy $(\rho_2-\rho_1)g(t) > 0$. The Richtmyer-Meshkov [2] (RM) instability occurs for an impulse $g = U\,\delta(t)$ from a shock and for all $\rho_2 \neq \rho_1$. The instabilities evolve through several stages [3] which are delineated by the amplitude h_k and wavelength $\lambda = 2\pi/k$ of the unstable modes. For $kh_k << 1$, the modes grow independently as $\exp(\gamma t)$ for RT and $\propto kUt$ for RM instabilities. When kh_k reaches some factor that depends on the spectral width [4-6], nonlinearities reduce the growth rates and broaden the spectrum. The interface then becomes asymmetric because spikes fall (heavy into light fluid) faster than bubbles rise (light into heavy fluid). If the instability is broadband, the nonlinearities will eventually produce a turbulent mixing layer.

The fate of the RT instability can be characterized by its bandwidth and duration. The bandwidth (k) determines the spatial complexity of the mixing zone and it is large when the system size L greatly exceeds the fastest growing wavelength λ_f. (When λ_f is determined by viscosity, this criterion is equivalent to having a large Reynolds number.) The duration determines the degree of nonlinearity and is characterized by $1/\gamma$ in the linear regime and a related scale evolution time in the nonlinear regime. Figure 1 shows γt vs λ for various physical systems that exhibit hydrodynamic instability. These include the explosion of supernovae [7-8] and magnetized plasmas [9-14], magnetic confinement [15, 16] and solar layers [17], inertial confinement fusion [18, 19] (ICF), the acceleration of metal plates [20-22], underground salt domes [23] and volcanic island arcs [24]. Since the instabilities are manifested in the nonlinear stages within complex physics environments, they are usually described with numerical simulations [5, 6, 25-33] (NS) and semi-empirical theories [34-39]. Here, we describe experiments to investigate the hydrodynamic instabilities in two interesting and difficult limiting regimes which are exemplified by natural phenomena.

In supernovae explosions, a strong outgoing shock produces density gradients at the concentration interfaces and excites the RM instability. The interfaces are then RT unstable as they decelerate $g \sim 20g_o$ ($g_o = 9.8$ m/s^2) against the overlying material. The mixing becomes highly turbulent because of the wide range in scales (100:1) and many e-foldings (30). Here, realistic experiments with sufficient diagnostic clarity are energetically prohibitive. (This differs from ICF in which the outward flow at the ablation surface stabilizes the usually virulent short wavelength modes and limits the instability to < 7 e-foldings.) However, scaled hydrodynamics experiments are possible since the plasma is Boltzman and can be replaced with a classical fluid. Indeed, there is a mathematical similarity between the interchange and RT instabilities when the plasma and magnetic field are replaced by heavy and light fluids, respectively. This analogy has motivated RT experiments [40-46] with Newtonian fluids that become quite turbulent because $L/\lambda_m > 100$ and $\gamma t \sim 50$ as indicated in Fig. 1 (LEM). They find self-similar mixing rates that can be used to test NS and empirical mix models, including those used in ICF [4, 5].

In geology, buried fluid layers of salt or lava can penetrate the denser overlayment to form underground salt domes [7] and volcanic islands [8]. Their regular spacings ($\lambda \sim 70$ km) and geological growth rates can be obtained from the RT dispersion by adjusting the thickness (H_i) and viscosities (ν_i) of the materials. However, this analysis infers geologically unrealistic values for H_1 and ν_2/ν_1 and cannot explain the absence of salt domes in more competent sedimentary strata [47]. These inconsistencies can be reconciled by including the shear modulus μ and tensile strength σ_o of the overlying material in the dispersion relation, but the affects are nonlinear and not understood. As a result, we conduct scaled experiments on the LEM using well characterized visco-elastic-plastic materials.

In this paper, we describe scaled experiments to investigate both turbulent mixing and the RT instability in elastic-plastic materials. In Sec. 2, we measure the turbulent RT growth rates with constant and impulsive accelerations over a comprehensive range of density ratios. In Sec. 3, the affects of compression on the RM growth rates are measured using strong radiatively driven shocks (Mach > 10). In

Sec. 4, critical wavelengths and amplitudes for RT instability is measured using a well characterized visco-elastic-plastic material.

2. Turbulent RT experiments with constant acceleration

In the asymptotic stage, the strong nonlinearities have long regulated the amplified initial scales leaving gt^2 as the lone dominant independent scale length. Short wavelength modes dissipate turbulent energy, but they do not significantly affect the instability growth. The mixing layer is found to grow self-similarly with amplitudes

$$h_i = \alpha_i A g t^2 \qquad (1).$$

where the index refers to the fluid being penetrated and $A = (\rho_2-\rho_1)/(\rho_2+\rho_1)$ is the Atwood number. Two amplitudes are required because spikes (i = 1) penetrate faster than bubbles (i = 2) asymptotically. The growth coefficients α_i have been obtained by experiments and NS for selected values of density ratio $R = \rho_1/\rho_2$, but the results are sparse and without consensus. For bubbles, α_2 appears to be independent of R with values ~ .04-.07 from experiments and α_2 ~ .03-.06 from NS. For spikes, α_1 increases from α_2 at R = 1 to α_1 ~ .5 (free fall) as $R \rightarrow \infty$, but the functional dependence on R is outstanding due to the paucity of data. Systematic measurements of α_i over a comprehensive range of R are required for testing NS and empirical mix models.

Here, we describe such measurements using the Linear Electric Motor [48] (LEM) and Newtonian fluids. For these experiments, the LEM provides a constant (± 5%) acceleration 30-70 g_o over a distance $Z \leq 1$ m and time $t \leq 55$ ms. The density ratio is varied $1.3 < R \leq 50$ using fluids that are incompressible, immiscible and inviscid. The container dimension L ~ 10 cm is much larger than the most unstable wavelength $\lambda_f < .5$ mm. From the calculation in Fig. 1 for R = 3, $50g_o$, and average surface tension 4 dyne/cm, the instability has sufficient bandwidth (100:1) and time ($50/\gamma$) to become trubulent. The large size also facilitates high quality diagnosis with laser induced fluoresence (LIF) and backlit photography (BP).

Sample images of RT mixing are shown in Fig. 2 for a constant acceleration. The top row shows a sequence of bilevel LIF images for R = 1.96 and g ~ 70 g_o. Bilevel images are obtained from the intensity images because the fluids are immiscible. The bottom row shows a series of BP images for R = 23.4 and g ~ 34 g_o. BP is used at large R because the fluids have different indeces of refraction and scatter light when emulsified. Thus, the mixing layer appears dark. The bubbles are observed [44-46] to coalesce as expected rom bubble competition [30, 49-52] but the spikes do not. These images are analyzed to obtain h_i as described in refs. [44-46].

The spatial evolution of h_i is shown in Fig. 3 for R = 1.96 and 23.4. The linear behavior is consistent with Eq. 1 since $gt^2 = 2Z$. The growth coefficients α_i are obtained with a linear least squares fit of h_i to Z with a zero offset to accomodate any initial perturbation [46]. Examples are indicated by the lines in Fig. 3.

The variation of α_i with Atwood number is shown in Fig. 4. The bubbles have an average value of $\alpha_2 \sim .053 \pm .006$ for A < .5 and $\alpha_2 \sim .049 \pm .003$ for A > .8. This slight downward trend indicated by the linear fit (line) is statistically marginal or may simply indicate some systematic experimental bias with A. For example, the scaled displacement AZ is larger for A ~ 1 and the experiment may be closer to an asymptotic self-similar state [14, 15] with lower α_2. Our values of α_2 lie between those measured previously with miscible [32, 33] (.04-.044) and immiscible [25, 40, 43] (~ .055-.075) fluids. For the spikes, α_1 remains within 20 % of α_2 for A < 0.5 and then it doubles as A increases 20% from .8 to .96. This behavior can be characterized as $\alpha_1 = .053\ R^{D\alpha}$ with $D_\alpha \sim 0.32$ as indicated by the solid line. The limited data of Youngs [13] (9 pts) and Kucherenko [34] (R = 20) yields an exponent of $D_\alpha \sim 0.2$. The discrepancy with the former data [13, 31] is due primarily to their 30% larger values of $\alpha_2 \sim .064$ for A > .8. Limited NS [Youngs, Freed] at R = 1.5, 3 and 20 give $D_\alpha \sim 1/4$ whereas mix models [Youngs, Alon, Glimm] yield $.3 < D_\alpha < .5$.

It is interesting to use our measurements of α_i in Eq. 1 to compare with the NS [8] of the explosion of SN1987A. The points in Fig. 5 represent the total width of the H-He and He-CO interfaces in

the 2D simulations. We estimate a deceleration ~ 20 g_o from the 1D velocity profiles and A ~ .6 from the 1D density profiles. The line is $h_1 + h_2$ using $\alpha_2 = .05$ and $\alpha_1 = .08$ is approximately three times smaller than the NS. This can be attributed to the threefold radial decompression observed in the 1D NS, which acts to expand the perturbations in excess of our incompressible results. However, the linear relationship in Fig. 5 shows that the mixing is self-similar as expected since the instability is broadband and nonlinear ($\gamma t > 10$).

3. Impulsive acceleration

An impulsive acceleration is interesting because it probes the inertial evolution of the hydrodynamic instabilities, which differs qualitatively from Eq. 1. In particular, consider an impulse $U = \int g\, dt$ in which g is applied for a short time t_o. The subsequent growth of a random (broadband) initial perturbation h_{io} is expected to be

$$h_i(t) = h_{io}\, \tau_i^{\theta_i} \qquad (2)$$

where $\tau_i \equiv V_{io}(t-t_o)/\theta_i h_{io} + 1$ and V_{io} is $V_i = dh_i/dt$ evaluated at $t = t_o$. Equation 2 has two key uncertainties. First, the variation of the exponents θ_i with density contrast is unclear because the few NS and experiments are not in accord. Second, when the impulse comes from a high Mach number shock, the compression of the densities (A) and initial amplitudes h_{io} complicates the evaluation of V_{io}.

In this section, we describe experiments to evaluate both issues using incompressible experiments on the LEM for (1) and using strong (Mach > 10) radiatively driven shocks on NOVA for (2).

Incompressible LEM experiments

The LEM experiments are similar to those described [46] in Sec. 2 except that the acceleration is increased in magnitude to ~ 150 g_o and shortened in duration t_o ~ 10 ms. This produces a net impulse of U ~ 1.5 cm/ms and initial displacement of $Z_o \sim gt_o^2/2$ ~ 7.5 cm. The

interface is initially RT unstable during the acceleration according to Eq. 1 producing h_{io} and V_{io}. This is followed by the power law behavior of Eq. 2 during the coast phase. This can be seen by plotting h_i vs Z in Fig. 6 for R = 2.83, 23.4, and 49.2. The experimental data (points) are fit (lines) to Eq. 2 by transforming time to $Z-Z_o = U(t-t_o)$ and adjusting h_{io} and θ_i. The inferred exponents indicated at each R indicate that θ_i are insensitive to R except for the spikes at R > 20.

The variation of θ_i with Atwood number is shown in Fig. 7. The bubble response is insensitive to A with a sample average of $\theta_2 = .25 \pm .005$. For the spikes, $\theta_1 \sim \theta_2$ out to A ~ 0.8 and then it increases dramatically to $\theta_1 = 1$ with considerable scatter $.35 < \theta_1 < .85$ for A ~ .92-.94. Here, we conducted many experiments with different fluid combinations and acceleration histories because there is a transition [20] in θ_1 expected near A = 0.9. This scatter may signify a sensitivity to initial conditions [18, 39]. As before, we fit the spike data to a power law $\theta_1 = \theta_2 R^{D_\theta}$ with $D_\theta \sim 0.21$ as indicated by the line in Fig. 7.

Our results lie in between previous experiments and calculations. Similar incompressible experiments [54] with liquids at R = 3 found smaller values $\theta_i \sim 0.1 \pm 0.02$ for both bubbles and spikes. The symmetry $\theta_1 \sim \theta_2$ is consistent with our experiments, but the values are ~ 50 % smaller. The NS of Alon *et al.*, [30] yield $\theta_1 = \theta_2 R^{D_\theta}$ with $D_\theta \sim 0.21$ similar to our experiments, but the values at small R are slightly larger $\theta_i = .4$. Different NS [25, 33] also obtain smaller exponents $\theta_i \leq .3$ whereas turbulence models obtain 1/3 [34] and < 2/3 [55]. More intimate comparisons between calculations and experiments are warranted because the differences in θ_i may partially be due to some sensitivity to initial conditions [25, 56].

Compressible NOVA experiments

When the unstable impulse is produced by a high Mach number shock, the initial conditions h_{io} and V_{io} are difficult to calculate because the shock compresses the material densities and interface. For example, when an incident shock of speed s_1 encounters a sudden density decrease, a backward rarefaction wave is generated in

addition to a transmitted shock of speed s_2. The compression reduces the pre-shock Atwood ratio A_- and amplitude h_{io-} to A and $h_{io} \sim h_{io-}(1-U/s_1)$. Analytical [57] and numerical [58] solutions for the linear growth rate with $A < 0$ can be estimated [59] by

$$V_{io} = AkU(h_{io}+h_{io-})/2 \qquad (3).$$

The solutions for $A >$ are different because the reflected wave is a shock [2, 58, 60]. The affect of compression is exemplified in Fig. 8 by plotting V_{io}/A_-kUh_{io-} vs the Mach number of the incident shock. The pre-shock densities are 1.7 and .12 g/cm^{-3} for fluids 1 and 2 with specific heat ratios 1.8 and 1.45. Thus, the growth rate decreases fivefold due to compression. The experimental data points are obtained on Nova with single mode 2D perturbations [61] of small amplitude. The growth rate is reduced further with a large intial amplitude [63] due to nonlinearities. Good agreement is obtained on single mode behavior among experiments, NS and theory [63].

Similar experiments [64] have been conducted with random 3D perturbations of amplitude $h_{io-} \sim 7$ μm and average wavelength $\lambda \sim 50$ μm. The shock and interface speeds are $s_1 \sim 46$ μm/ns, $s_2 \sim 73$ μm/ns and $U \sim 57$ μmns. The initial fluid densities 1.7 and .12 g/cm^{-3} were compressed to $\rho_1 \sim 2$ g/cm^{-3} and $\rho_2 \sim .5$ g/cm^{-3}, such that $A \sim -.6$. The variation of h_1+h_2 with the net displacement $Z-Z_o$ is shown in Fig. 9. The data is fit with to a power law with exponent $.5 \pm .1$, which is slightly larger but consistent with those obtained from the LEM. We do not currently understand this difference, but several possibilities exist. First, the laser drive decreases in time causing the densities to decompress and the interface to decelerate [65]. This causes the perturbations to expand like an accordian and introduces an RT component because $Ag > 0$. Both effects can significantly increase the inferred exponents. Second, the initial perturbations are more symmetric on Nova than on the LEM at $A = .6$, which may lead to different exponents if they are sensitive to initial conditions. These effects may also be important in other shock driven experiments [66-71] which exhibit large exponents 2/3-1, particularly since NS [25, 33] obtain exponents < .3.

4. RT instability in elastic-plastic materials

The nonlinear response of an elastic-plastic greatly affects the RT dispersion at short wavelengths [72-77]. At small amplitude, the elastic stress $-2\mu k^2 h_k$ can overcome the buoyancy $\delta\rho\ g k h_k$ and stabilize modes with

$$k > \delta\rho\ g/2\mu \equiv k_c \qquad (4)$$

where $\delta\rho = (\rho_2 - \rho_1)$. These modes may again be destabilized if the initial amplitude h_o is large enough that the pressure drop across the perturbation exceeds the tensile yield σ_o, namely,

$$P^* \equiv \delta\rho\ g\ h_o / 2\ \sigma_o \geq P_{cr} \qquad (5).$$

Various models [72-76] exist for the scaled critical pressure, but the most promising [77] appears to be

$$P_{cr} = (1-.86e^{-kH_2/\sqrt{3}})\ [(1-e^{-kH_2/\sqrt{3}})^2-(k_c/k)^2] \qquad (6)$$

for 2D perturbations where H_2 is the thickness of the elastic plate. Ehanced stability is predicted [75] in 3D with $P_{cr} \sim 2$.

The amplitude threshold for instability has been observed with strong materials (metals) using high explosives (HE) drivers. However, the theoretical interpretation is not unambiguous because the dynamical state or properties of the material at the ~ 100 kbar pressure are not measured independently. In addition, inhibited growth can be mis-interpreted as stability because the experimental duration is short $< 2/\gamma$. Here, we summarize scaled experiments [78] on the LEM lasting $15/\gamma$ with yogurt as the elastic-plastic material. The constitutive properties ($\mu \sim 1500 \pm 300$ Pa, $\sigma_o = 315 \pm 60$ Pa, and $\nu = 5 \pm 1.5$ Pa-s) are measured [79] independently under experimental conditions using elastic waves and uniaxial compression and extension tests.

The existence of a critical wavelength and amplitude for instability is demonstrated in Fig. 10. The yogurt (opaque) is outlined by the dashed line and has dimensions L_x = 6 cm, L_y = 6.3 cm and H_2 = 3.2 cm. The light fluid is compressed nitrogen (2 10^5 Pa). In the first row, the interface is flat and g is increased until $\lambda_c = 4\pi\mu/\delta\rho\, g$ is made small enough to fit into the container. Indeed, the instability is observed for $g \geq 53\ g_o$, which is near the threshold $43 \pm 8\ g_o$ obtained from setting $L_x^{-2} + L_y^{-2} = \lambda_c^{-2}$. The critical wavelength has not been measured with HE because the plate width ($< \lambda_c$) was too small. In the second row, 2D perturbations are imposed with increasing amplitudes h_o at λ = 3 cm. With $g = 28\ g_o$, we have λ_c = 6.7 cm > λ and RT stability until the amplitude threshold is exceeded for $h_o \geq 1.2$ mm. The temporal evolution for h_1 is shown in Fig. 10b for different h_o. For $h_o <$ 1.2 mm, the perturabtions stretch elastically but they are stable and recover following the acceleration. For $h_o >$ 1.2 mm, the amplitude grows exponentially with $\gamma \sim 100\ s^{-1}$ consistent with linear theory with viscosity. There is a time delay to the exponential phase which decreases as h_o increases above the threshold.

Equation 6 is tested by measuring the amplitude threshold at different accelerations and plotting P^* against $\lambda/\lambda_c = \lambda g\ \delta\rho/4\pi\mu$ as shown in Fig. 11a. The solid circles are measured with H_2 = 3.2 cm and 2D perturbations with λ = 3 cm and various values of h_o similar to Fig. 10. These are in good agreement with Eq. 5 (line) and show the steady decrase in the critical amplitude as λ approaches λ_c. The competing models [72, 75] predict a larger and constant $P_{cr} \sim 1$ independent of $\lambda < \lambda_c$. Similar experiments with 3D perturbations [78] confirm the enhanced stability.

These results bear directly on the geophysical systems because the earth's lithosphere has both elastic and plastic characteristics [80-82]. At a temperature1300° C and confining pressure 300 MPa representative of the magma source, olivine has characteristic values of $\sigma_o \sim 210^8$ dyne/cm^2, $\mu \sim 10^{10}$ dyne/cm^2 and $\rho_2 \sim 3$ g/cm^3. The andesite magma has $\rho_1 \sim 2.5$ g/cm^3, which makes $\lambda_c \sim 10^4$ km >> $\lambda \sim$ 70 km and $2\sigma_o/\delta\rho g_o \sim 8$ km. This means that the RT instability is inhibited until P_{cr} can be reduced significantly. Evaluating Eq. 5 with

$\lambda << \lambda_c$ in Fig. 11b, we find that P_{cr} is decreasing for $\lambda > H_2 \geq 40$ km, which is near the minimum observed spacing for volcanic islands. Such an interpretation links the observed spacing with the thickness of the lithosphere. At the average spacing of $\lambda \sim 70$ km, the critical amplitude is estimated to be 5-6 km, which is about 10% of the depth of the magma source. This appears to be somewhat large and better modelling is required to include the substantial variations with depth.

In previous calculations, the fluids were characterized simply as viscous with a peak growth rate at $\lambda \sim \pi H_1(\nu_2/\nu_1)^{1/3}$. This led to an unreasonably thin (< 50 m) magma source for characteristic viscosity ratios of $\nu_2/\nu_1 < 10^{15}$. Such a viscosity model may be more representative of salt domes where the overlying material has negligible strength. However, even here, the viscosity model implies source thicknesses are small and cannot explain the absence of salt domes in more competent sedimentary strata.

5. Summary and discussion

We have presented a series of experiments to investigate the nonlinear evolution of the RT and RM instabilities.

For a constant acceleration, the RT instability is found to grow self-similarly according to Eq. 1. The growth coefficients α_i are measured over a comprehensive range of density ratio and the results are found applicable to supernova exlposions.

For an impulsive acceleration, there are two components. The RM impulse from a shock is greatly reduced at high Mach number due to compressive effects in reasonable agreement with linear theory. The ensuing motion is essentially imcompressible describable by a power law of Eq. 2. However, the exponents obtained from the compressible RM experiments are larger than those obtained from incompressible RT experiments. The discrepancy is currently not understood.

The affect of non-Newtonian constitutive properties on the RT instability was investigated with scaled experiments of long duration ($15/\gamma$) and well characterized material properties. We observe a critical wavelength and amplitude for instability associated with the

shear modulus and tensile yield of the material. The results are directly applicable to geophysical flows subject to the RT instability.

Acknowledgments

We thank M. Schneider, D. Youngs, R. Gore, A. Velikovich, E. Burke, B. Remington, J. Grove, R. Holmes, D. Sharp, K. Mikaelian, D. Shvarts, J. Glimm, J. Colvin and C. Frerking for invaluable contributions. We also appreciate the support of M. E. Eckart and J. D. Kilkenny. This work was performed under the auspices of the U.S. Department of Energy by the Lawrence Livermore National Laboratory under Contract No. W-7405-ENG-48.

List of References

[1] Lord Rayleigh, Scientific Papers **II**, 200, Cambridge, England, 1900. G. I. Taylor, Proc. Roy. Soc. London **A201**, 192 (1950).

[2] R.D. Richtmyer, Commun. Pure Appl. Math. **13**, 297 (1960). E.E. Meshkov, Izv. Acad. Sci. USSR Fluid Dynamics **4**, 101 (1969).

[3] D.H. Sharp, Physica **12D**, 3 (1984)

[4] Steven W. Haan, *et al.*, Phys. Fluids B **3**, 2349 (1991)

[5] D. Shvarts, *et al.*, Phys. Plasmas **2**, 2465 (1995)

[6] M. M. Marinak *et al.*, Phys. Rev. Lett. **80**, 4426 (1998)

[7] W. David Arnett *et al.*, Annu. Rev. Astron. Astrophys. **27**, 629 (1989)

[8] E. Muller, B. Fryxell, and D. Arnett, Astron. Astrophys. **251**, 505 (1991)

[9] S. Okada, K. Sato and T. Sekiguchi, J. Appl. Phys. **20**, 157 (1981)

[10] B. H. Ripin *et al.*, Phys. Rev. Lett. **59**, 2299 (1987)

[11] Guy Dimonte and L. G. Wiley, Phys. Rev. Lett. **67**, 1755 (1991)

[12] P. A. Bernhardt *et al.*, J. Geophys. Res. **92**, 5777 (1987).

[13] M. F. Thomsen *et al.*, J. Geophys. Res. **91**, 2961 (1986)

[14] J. D. Huba, A. B. Hassam and D. Winske, Phys. Fluids B **2**, 1676 (1990)

[15] M.N. Rosenbluth and C.L. Longmire, Annals Phys. **1**, 120 (1957)

[16] John R. Ferron *et al.*, Phys. Fluids **26**, 2227 (1983)

[17] F. Cattaneo and D.W. Hughes, J. Fluid Mech. **196**, 323 (1988)

[18] J. D. Lindl and W. C. Mead, Phys. Rev. Lett. **34**, 1273 (1975). H. Sakagami and K. Nishikara, Phys. Fluids **B2**, 2715 (1990). J. D. Kilkenny *et al.*, Phys. Plasmas **1**, 1379 (1994). B. A. Remington *et al.*, Phys. Plasmas **2**, 241 (1995).

[19] V. A. Andronov, S. M. Bakhrakh, V. N. Mokohov, V. V. Nikiforov, and A. V. Pevnitskii, JETP Lett. **29**, 56 (1979).

[20] John F. Barnes *et al.*, J. Appl. Phys. **45**, 727 (1974); *ibid.*, **51**, 4678 (1980).

[21] A. I. Lebedev *et al.*, Physics-Doklady **41**, 328 (1996).

[22] J. Degnan *et al.*, Phys. Rev. Lett. **74**, 98 (1995).

[23] Franz Selig and E.G. Wermund, Geophys. **32**, 726 (1966)

[24] B. D. Marsh, J. Geology **87**, 687 (1979)

[25] D. L. Youngs, Laser and Particle Beams **12**, 725 (1994);Phys. Fluids **A 3**, 1312 (1991); Physica **D 37**, 270 (1989); Physica **12D**, 32 (1984)
[26] J. Glimm, *et al* ., Phys. Fluids **A 2**, 2046 (1990)
[27] N. Freed,*et al.*, Phys. Fluids **A 3**, 912 (1991)
[28] X. L. Li, Phys. Fluids **A 5**, 1904 (1993)
[29] P.F. Linden, J.M. Redondo, and D.L.Youngs, J. Fluid Mech. **265**, 97, (1994)
[30] U. Alon *et al.*, Phys. Rev. Lett. **74**, 534 (1995)
[31] J. Hecht *et al.*, Laser and Particle Beams **13**, 423 (1995)
[32] Catherine Cherfills and Karnig O. Mikaelian, Phys. Fluids **8**,522 (1996)
[33] T. Pham and D.I. Meiron, Phys. Fluids A **5,** 344 (1993)
[34] S. Gauthier and M. Bonnet, Phys. Fluids A **2**, 1685 (1990).
[35] J.C. Hanson *et al.*, Laser and Particle Beams **8**, 51 (1990).
[36] Nathan Freed *et al.*, Phys. Fluids **A 3**, 912 (1991)
[37] Jacob Hecht, Uri Alon, Dov Shvarts, Phys. Fluids **6**, 4019 (1994)
[38] Yupin Chen, James Glimm, David A. Sharp, Phys. Fluids **8**, 816 (1996)
[39] James Glimm, David Saltz, David H. Sharp, Phys. Rev. Lett. **80**, 712 (1998)
[40] K.I. Read, Physica **12D**, 45 (1984)
[41] M.J. Andrews and D.B. Spalding, Phys. Fluids **A 2**, 922 (1990)
[42] P.F. Linden and J.M. Redondo, Phys. Fluids **A 3**, 1269 (1991)
[43] Yu. A Kucherenko, *et al.*, Proceedings of Third Int. Workshop on Physics Compressible Turbulent Mixing, R. Dautray, ed. (Abbey of Royaumont, France, 1991), p. 427.
[44] Guy Dimonte and Marilyn Schneider, Phys. Rev. E **54**, 3740 (1996)
[45] Marilyn Schneider, Guy Dimonte and Bruce Remington, Phys. Rev. Lett. **80**, 3507 (1998)
[46] Guy Dimonte and Marilyn Schneider, submitted to Phys. Fluids 1998
[47] L.L. Nettleton, Bull. Amer. Assoc. Petroleum Geol. **27**, 51 (1943)
[48] Guy Dimonte, *et al.*, Rev. Sci. Inst. **67**, 302 (1996)
[49] D. Layzer, Astrophysical J. **122**, 1 (1955)
[50] J. A. Zufiria, Phys. Fluids **31**, 440 (1988)

[51] J. Glimm and X.L. Li, Phys. Fluids **31**, 2077 (1988)
[52] X.L. Li, Phys. Fluids **8**, 336 (1996)
[53] D.L. Youngs, in Advances Compressible Turbulent Mixing, ed. W.P. Dannevik, A.C. Buckingham, and C.E. Leith (Princeton U., Princeton, NJ, 1992), p. 607, Conf-8810234
[54] Yu. A Kucherenko, *et al.*, Laser and Particle Beams **15**, 25 (1997)
[55] G.I.Barenblatt, in **Nonlinear Dynamics and Turbulence**, eds. G.I. Barenblatt, G. Ioos, and D.D. Joseph, Pitman, Boston, 1983, p. 48.
[56] Qiang Zhang, Phys. Rev. Lett. **81**, 3391 (1998)
[57] Alexander L. Velikovich, Phys. Fluids **8**, 1666 (1996)
[58] Y. Yang, Q. Zhang and D.H. Sharp, Phys. Fluids **6**, 1856 (1994)
[59] K.A. Meyer and P.J. Blewett, Phys. Fluids **15**, 753 (1972)
[60] G. Fraley, Phys. Fluids **29**, 376 (1986)
[61] Guy Dimonte, *et al.*, Phys. Plasmas **3**, 614 (1996); Guy Dimonte and Bruce Remington, Phys. Rev. Lett. **70**, 1806 (1993).
[62] Alexander L. Velikovich and Guy Dimonte, Phys. Rev. Lett. **76**, 3112 (1996)
[63] R. Holmes *et al.*, (accepted for publication J. Fluid Mech., 1998)
[64] Guy Dimonte, C.E. Frerking, and Marilyn Schneider, Phys. Rev. Lett. **74**, 4855 (1995); Guy Dimonte and Marilyn Schneider, Phys. Plasmas **4**, 4347 (1997)
[65] Jeff Colvin (private communication, 1998)
[66] D.R. Farley, *et al.*, Proceedings of Sixth Int. Workshop on Physics Compressible Turbulent Mixing, G. Jourdan and L. Houas, eds. (Marseille, France, 1997), p. 161.
[67] V. A. Andronov*et al.*, Sov. Phys. JETP **44**, 424 (1976)
[68] S. G. Zaitsev*et al.*, Sov. Phys. Dokl. **30**, 579 (1985)
[69] M. Brouillette and B. Sturtevant, Phys. Fluids A **5**, 916 (1993)
[70] M. Vetter and B. Sturtevant, Shock Waves **4**, 247 (1995)
[71] L. Houas and I. Chemouni, Phys. Fluids **8**, 614 (1996)
[72] J. W. Miles, General Dynamics Report No. GAMD-7335, AD643161 (1966) (unpublished)
[73] A. C. Robinson and J. W. Swegle, J. Appl. Phys. **66**, 2859 (1989)
[74] J. W. Swegle and A. C. Robinson, J. Appl. Phys. **66**, 2838 (1989)

[75] D. C. Drucker, **Mechanics Today**, edited by S. Nemat-Nasser (Permagon , Oxford (1980), Vol. 5, p. 37
[76] E. L. Ruden and D. E. Bell, J. Appl. Phys. **82**, 163 (1997)
[77] P. N. Nizovtsev and V. A. Raevskii, VANT Ser. Teor. Prikl. Fizika No. 3, 11 (1991) (in Russian)
[78] Guy Dimonte, Rob Gore, and Marilyn Schneider, Phys. Rev. Lett. **80**, 1212 (1998)
[79] Guy Dimonte, *et al.*, J. Rheol. **42**, 727 (1998)
[80] W. Spence, J. Geo. Res. **82**, 213 (1977)
[81] Herbert E. Huppert, J. Fluid Mech. **173**, 557 (1986)
[82] David L. Kohlstedt and Prame N. Chopra, in **Magmatic Systems**, ed. M.P. Ryan, Academic Press, San Diego, CA 1994, pp. 37-53

Figure Captions

Figure 1: Number of RT e-foldings vs wavelength for various physical systems.

Figure 2: (a) Laser induced fluoresence images at various displacements for density ratio R = 1.96 and a constant g = 70 g_o. (b) Backlit photography images for R = 23.4 and g = 34 g_o. The initial interfaces are marked by arrows and the horizontal widths are (a) 6.2 cm and (b) 6.7 cm.

Figure 3: Spatial variation of bubble and spike amplitudes for constant accelerations. Points are data and lines are linear fits to obtain the growth coefficients α_i.

Figure 4: Growth coefficients α_i for bubbles and spikes vs Atwood number. Points are data and lines are fits.

Figure 5: Total mix width at He-H and CO-He interfaces vs deceleration distance gt^2 for supernova 1987A. Points are obtained from simulation in ref. [8] and line is Eq. 1 using the measured α_i at A = .6.

Figure 6: Spatial evolution of bubble and spike amplitudes for pulsed accelerations. Points are data and lines are fits following the impulse using Eq. 2 for the exponents θ_i as indicated.

Figure 7: Power law exponents θ_i for bubbles and spikes vs Atwood number. Points are data and lines are fits.

Figure 8: RM linear growth rates scaled to the incompressible growth rate vs Mach number of incident shock. Points represent measurements in ref. [ ] and line is calculated from Eq. 3 and ref. [ ] for R = .068 and adiabatic constants 1.8 and 1.45 for fluids 1 and 2.

Figure 9: Total mix width vs the displacement of the interface for random 3D imposed perturbations. Incident shock has Mach > 10 and fluids have R = .064 and adiabatic constants 1.8 and 1.45 for 1 and 2. Lines are fits with $\theta_i = .5 \pm .1$.

Figure 10: Temporal variations of spike amplitude and associated images for constant accelerations (dashed lines). (a) The interface is flat and the magnitude of g is increased until instability is observed for yogurt at 53 g_o. The Newtonian fluid (+) is always unstable. (b) Perturbations of various amplitudes are imposed with λ = 3 cm and g = 28 g_o. The instability transition occurs at 1.2 mm.

Figure 11: Critical scaled pressure (amplitude) for instability. (a) Experimental points are taken with different values of g and the line is Eq. 6 with λ = 3 cm and H_2 = 3.2 cm. (b) Eq. 6 for λ_c = infinity.

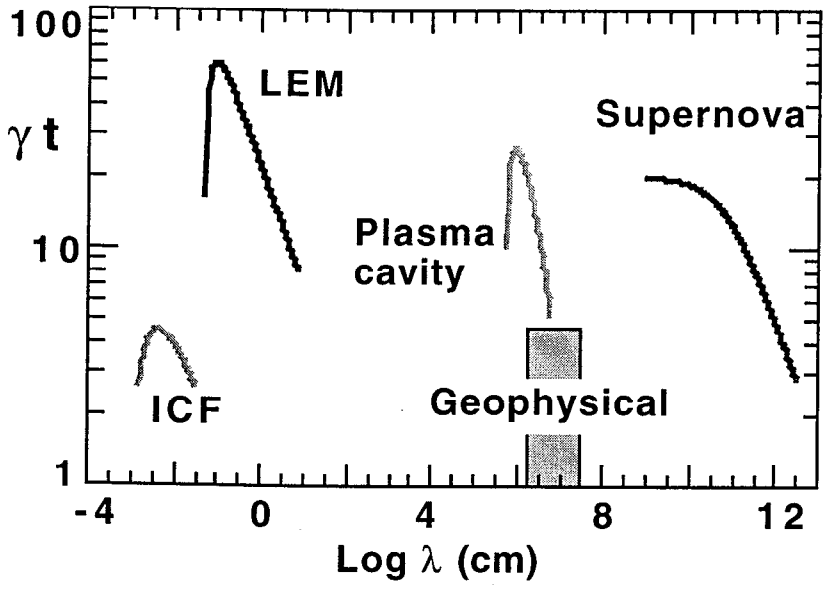
100
γ t
10
1
LEM
Supernova
Plasma
cavity
ICF
Geophysical
-4
0
4
8
12
Log λ (cm)

APS_Fig_01

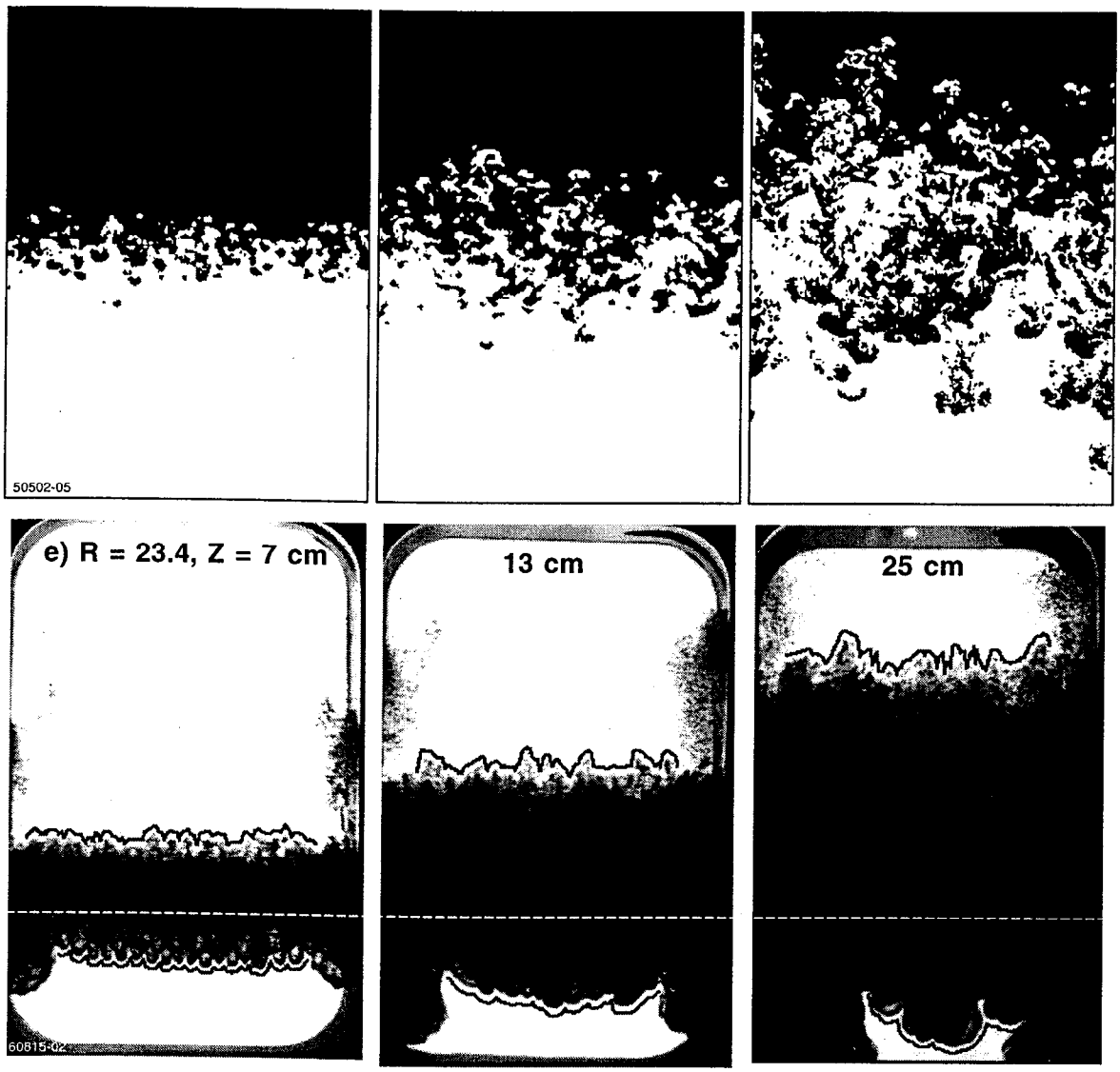
50502-05
e) R = 23.4, Z = 7 cm
13 cm
25 cm
60615-02

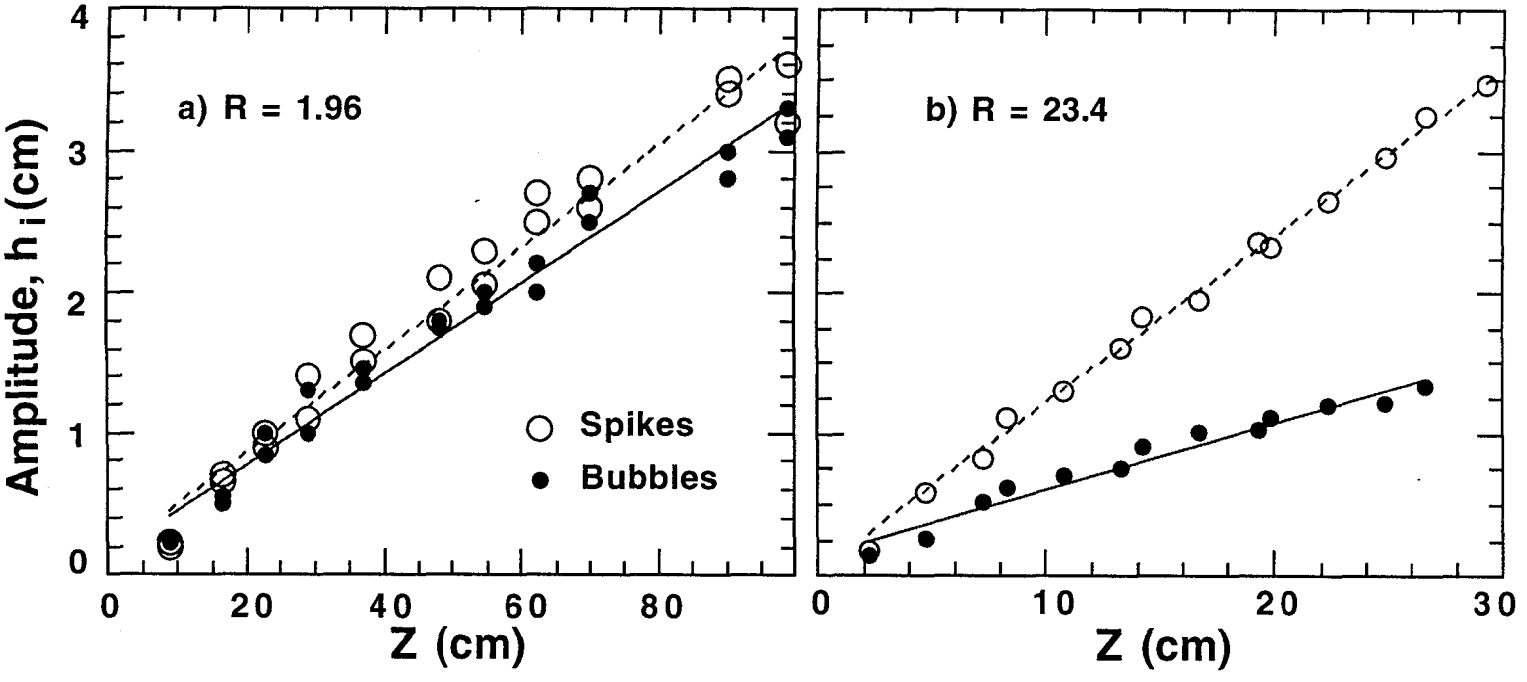
a) R = 1.96
b) R = 23.4
Spikes
Bubbles
Amplitude, h i (cm)
Z (cm)
Z (cm)
0
1
2
3
4
0
20
40
60
80
0
10
20
30

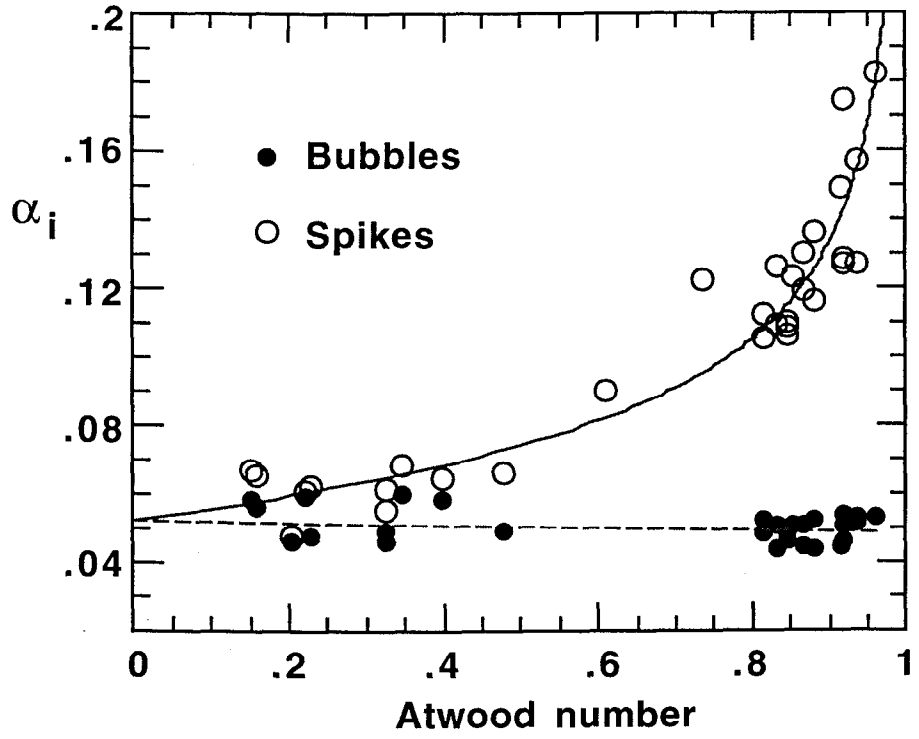

APS_Fig_04

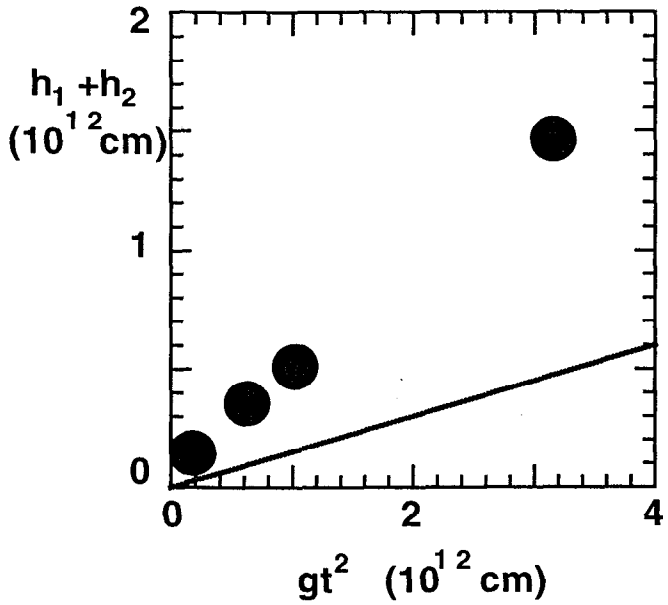

APS_Fig_05

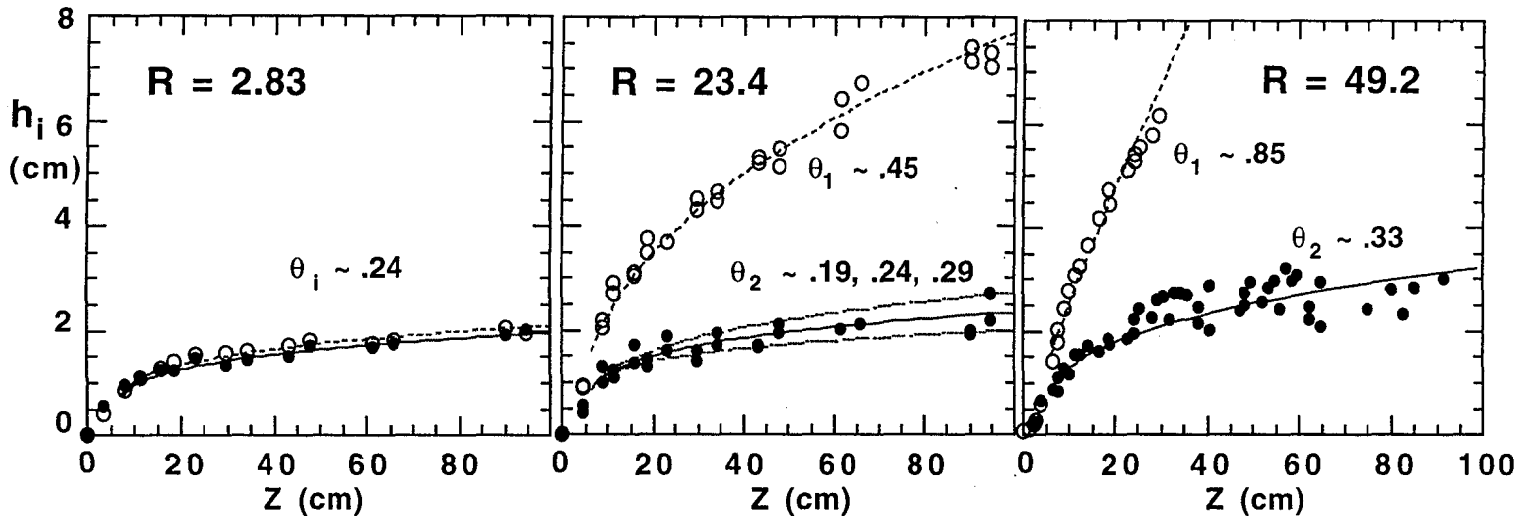
R = 2.83
R = 23.4
R = 49.2
h_i 6 (cm)
8
4
2
0
θ_i ~ .24
θ_1 ~ .45
θ_2 ~ .19, .24, .29
θ_1 ~ .85
θ_2 ~ .33
0 20 40 60 80
0 20 40 60 80
0 20 40 60 80 100
Z (cm)
Z (cm)
Z (cm)

APS_Fig_07

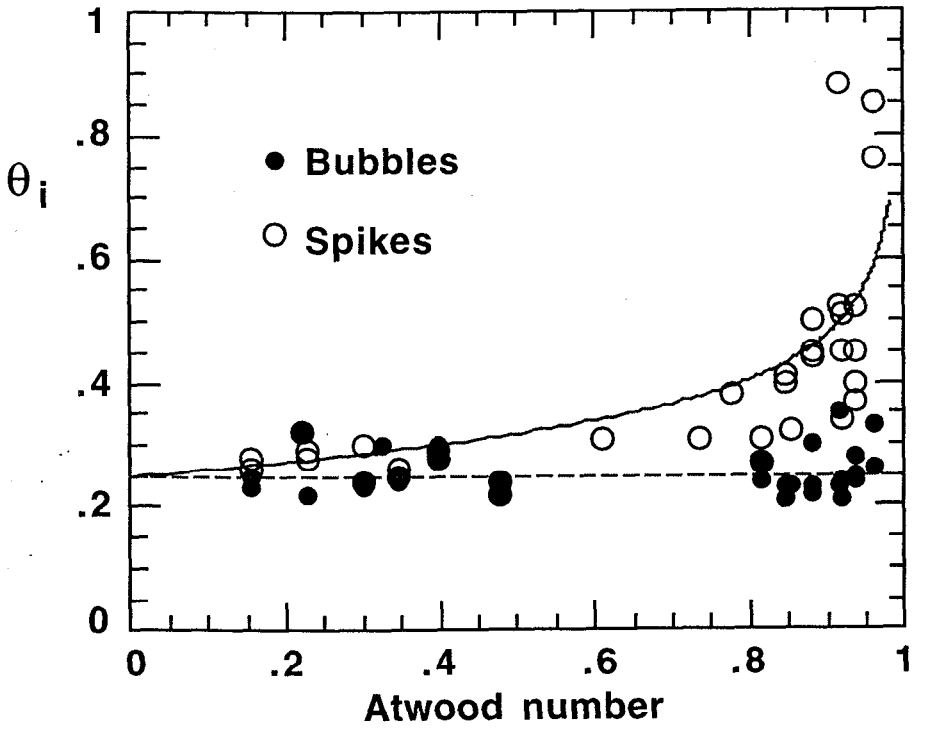
1
.8
.6
.4
.2
0
θ_i
Bubbles
Spikes
0
.2
.4
.6
.8
1
Atwood number

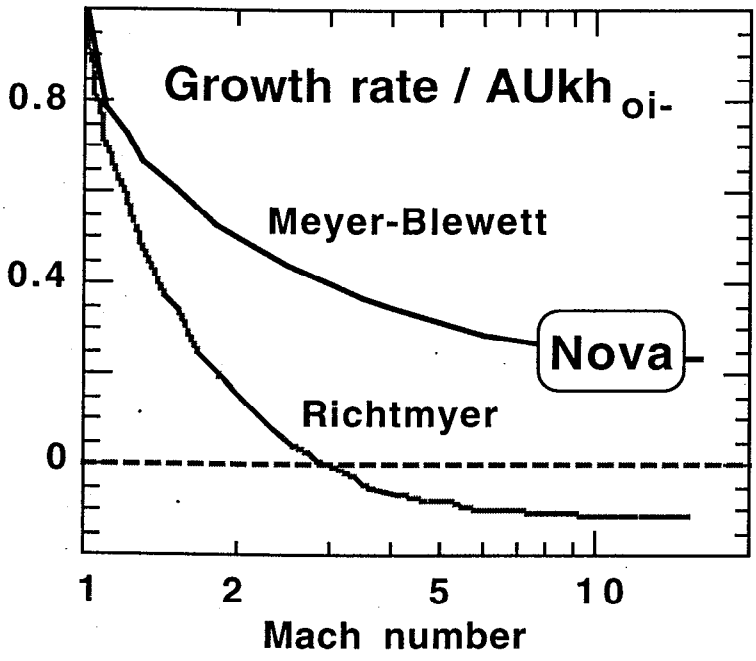
Growth rate / AUkh oi-
0.8
0.4
0
Meyer-Blewett
Nova
Richtmyer
1
2
5
10
Mach number

APS_Fig_08

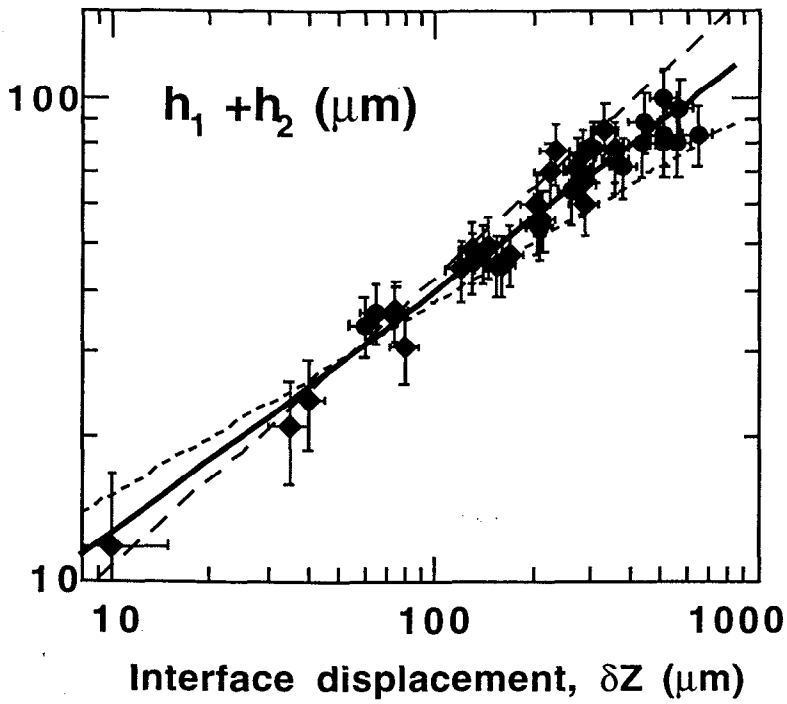

APS_Fig_09

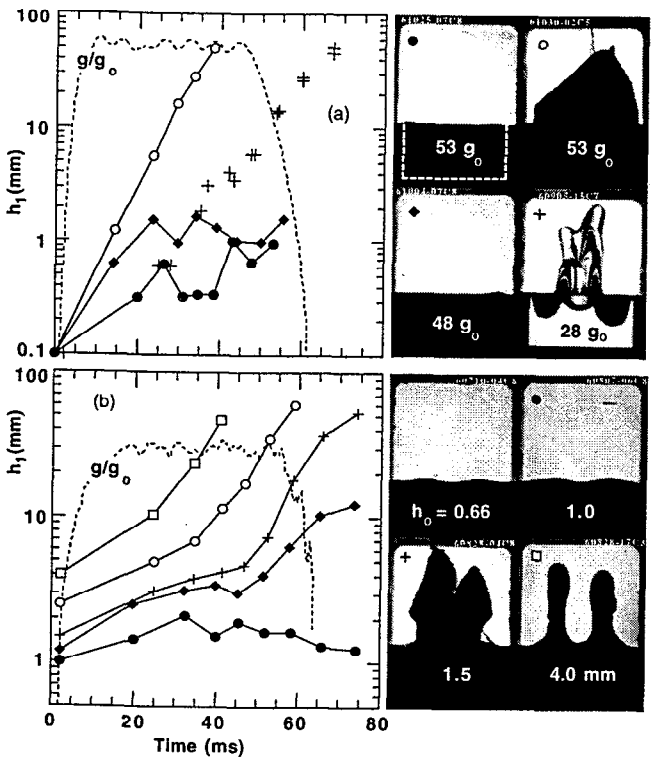
100
10
1
0.1
h_1(mm)
g/g$_o$
(a)
53 g$_o$
53 g$_o$
48 g$_o$
28 g$_o$
100
10
1
h_1(mm)
(b)
g/g$_o$
h_o = 0.66
1.0
1.5
4.0 mm
0
20
40
60
80
Time (ms)

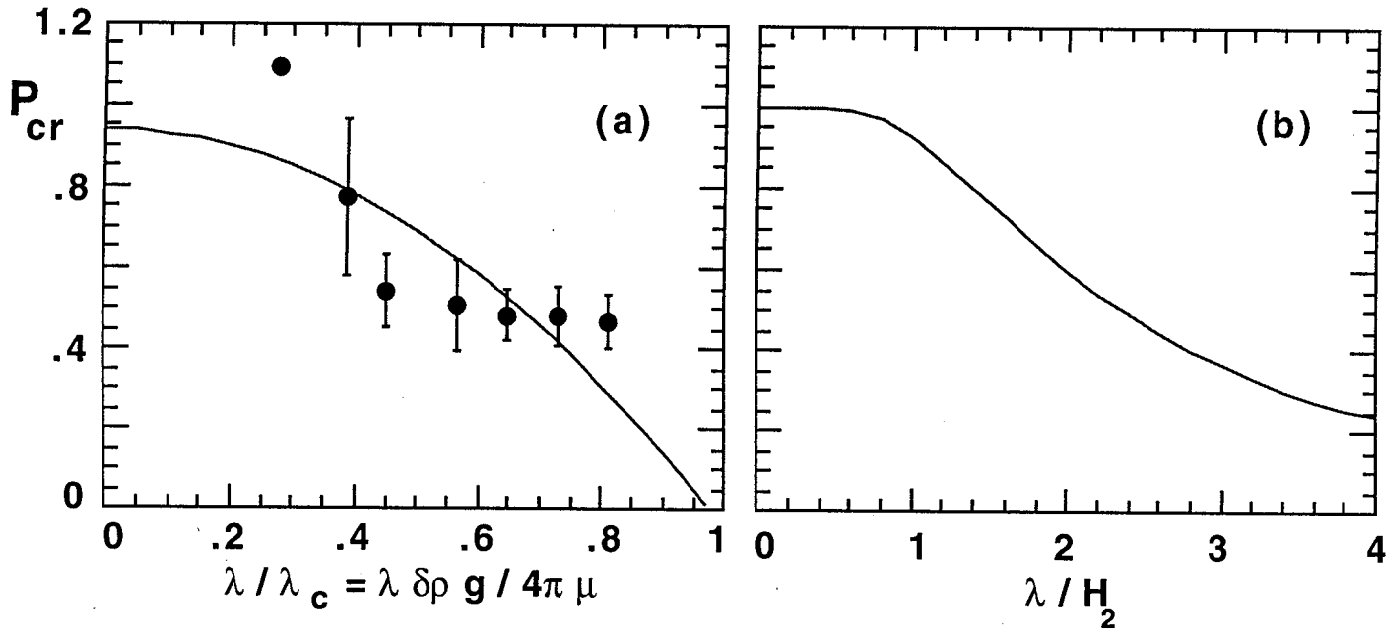
1.2
P_{cr}
.8
.4
0
(a)
0
.2
.4
.6
.8
1
$\lambda / \lambda_c = \lambda\, \delta\rho\, g / 4\pi\, \mu$
(b)
0
1
2
3
4
λ / H_2

APS_Fig_11